PCCP

PAPER

View Article Online
View Journal | View Issue

Cite this: *Phys. Chem. Chem. Phys.*, 2025, **27**, 17548

Photochemistry of dibromine peroxide, BrOOBr

Wiem Chebbi, *[ab] Najoua Derbel, [ac] Thibaud Cours [b] and Alexander Alijah [b]

Received 5th June 2025,
Accepted 15th July 2025

DOI: 10.1039/d5cp02124c

rsc.li/pccp

The photochemistry of dibromine peroxide was investigated by means of mixed quantum–classical trajectory calculations on seven coupled potential energy surfaces. Photoexcited BrOOBr disintegrates rapidly, at a rate comparable with thermal decomposition. The rate constant is $J = 9.7 \times 10^{-2}$ s^{-1}. The mechanism was investigated, and the final photolysis products are shown to be mainly 2Br + O_2, though there is a minor channel leading to 2BrO. Their formation involves an unusual intermolecular vibronic energy redistribution process. A hitherto unknown isomer of BrOOBr, the van der Waals complex $O_2(a^1\Delta_g)\cdot Br_2(X^1\Sigma_g^+)$, was found, which is more stable than the peroxide by 1.2 mE_h.

1. Introduction

Free halogen atoms and halogen oxides are mainly responsible for the depletion of stratospheric ozone by converting it into dioxygen. Evidence for a catalytic cycle involving chlorine atoms, which are created in the stratosphere by photochemical decomposition of halogenated aliphatic hydrocarbons, was first provided by Molina and Rowland.[1] Chlorine oxide appears as an intermediate in this cycle. Chlorine oxide also contributes to other catalytic cycles, such as to the ClO dimer cycle:[2]

$$\begin{gathered} 2(X + O_3 \rightarrow XO + O_2) \\ 2XO + M \rightleftharpoons XOOX + M \\ \underline{XOOX + h\nu \rightarrow 2X + O_2} \\ 2O_3 \rightarrow 3O_2 \end{gathered} \quad (1)$$

with X = Cl. Other more effective cycles are the XO/HO_x cycle and the XO/NO_x cycle, which are well documented in the literature.[3–5] Bromine, though less abundant, has up to sixty times higher ozone-depleting efficiency compared to chlorine,[6] which is expressed by the α-factor.[7–9] Furthermore, the proportion of bromine present in radical active forms (Br and BrO) seems higher than the equivalent proportion of chlorine.[10,11] Thus, it has been estimated that bromine compounds released from anthropogenic and natural sources may finally lead to 25% of the total ozone depletion in the Antarctic stratosphere and up to 40% of the loss in the Arctic.[12,13] Bromine mainly acts through the mixed BrO/ClO dimer cycle[14] and the BrO/HO_2 cycle,[4] and to a minor extent through the BrO dimer cycle. However, the latter is important in the troposphere, especially in the Arctic marine boundary layer in early spring, when BrO concentrations are relatively high.[15] Of the other halogens, only iodine plays a major role.[16,17] Fluorine has no ozone-depleting potential, as any fluorine atoms released from fluorine species such as CFCs will be converted into stable hydrogen fluoride, HF.[18,19]

Understanding the photochemistry of halogen oxides, and in particular bromine oxides, is of great importance given their ozone-destroying capacity. In the present work, we examine the photochemistry of dibromine peroxide, BrOOBr, which is formed in the BrO dimer cycle. The kinetics of the BrO + BrO reaction was studied experimentally by a large number of groups[20–36] since the 1970s. In the experiments, BrO was produced by flash photolysis[37] of a mixture of Br_2, O_2 and O_3 and the products were identified by methods such as UV spectroscopy and molecular beam mass spectrometry. The reaction is believed to proceed *via* the following mechanism, first suggested by Sander and Watson,[22] and involves the following three channels:

channel a:

$$\begin{gathered} BrO + BrO \rightleftharpoons BrOOBr^* \\ BrOOBr^* \rightarrow BrOO + Br \\ BrOO \rightarrow O_2 + Br \\ \overline{BrO + BrO \rightarrow O_2 + 2Br} \end{gathered} \quad (2)$$

[a] *LSAMA, Laboratoire de Spectroscopie Atomique Moléculaire et Applications, Department of Physics, University Tunis – El Manar, 1060 Tunis, Tunisia*
[b] *GSMA, Groupe de Spectrométrie Moléculaire et Atmosphérique, UMR CNRS 7331, University of Reims Champagne-Ardenne, 51100 Reims, France. E-mail: wiem.chebbi@univ-reims.fr*
[c] *FSB, Faculty of Sciences of Bizerte, University of Carthage, 7021 Jarzouna – Bizerte, Tunisia*

channel b:

$$\mathrm{BrO} + \mathrm{BrO} \rightleftharpoons \mathrm{BrOOBr}^* \qquad \mathrm{BrOOBr}^* \rightarrow \begin{array}{c}\mathrm{Br}\quad\quad\mathrm{Br}\\ \diagdown\quad\diagup\\ \mathrm{O}\quad\mathrm{O}\end{array} \rightarrow \mathrm{Br_2} + \mathrm{O_2} \tag{3}$$

channel c:

$$\mathrm{BrO} + \mathrm{BrO} \rightleftharpoons \mathrm{BrOOBr}^* \qquad \mathrm{BrOOBr}^* + \mathrm{M} \rightarrow \mathrm{BrOOBr} + \mathrm{M} \tag{4}$$

The JPL-recommended[38] rate constants for the two bimolecular reactions are $k_{1a} = 2.4 \times 10^{-12} \exp(40/T)$ cm^3 molecule^{-1} s^{-1} and $k_{1b} = 2.8 \times 10^{-14} \exp(860/T)$ cm^3 molecule^{-1} s^{-1}. An estimate exists[33] for the termolecular rate constant, k_{1c}. In fact, there are two experimental papers that provide evidence for a short-lived intermediate species. The first is that of Mauldin *et al.*[27] who, in 1993, studied this reaction at 220 K. A species bound by at least 5 kcal mol^{-1}, attributed to BrOOBr, was observed at 312 nm. Five years later, Harwood and colleagues[33] again studied this reaction. At low temperatures, 222 K and 235 K, they also observed the presence of an UV absorber other than BrO, O_3 or Br_2, which was identified as BrOOBr. Simulations of the overall BrO loss reaction showed that inclusion of the formation and thermal decomposition of BrOOBr accurately described the observed data. The best fit was obtained with a Br_2O_2 absorption cross-section of 1.2×10^{-17} cm^2 molecule^{-1} at 320 nm. Based on this value, the UV spectrum was scaled accordingly. It compares well with the residual UV spectrum obtained by Mauldin *et al.* The rate constants for the formation and thermal decomposition of BrOOBr show that this species can only exist at low temperatures, below 250 K. The other proposed intermediates, bromine peroxide, BrOO, and the trapezoidal Br_2O_2 complex were not observed.

The structures and stability of dibromine peroxide, BrOOBr, and its isomers were investigated computationally[39–46] at both DFT and *ab initio* levels of theory. It was found that three isomers with the formula Br_2O_2 exist, which are, in order of decreasing stability, dibromine peroxide, BrOOBr, bromyl bromide, BrBrO(O), and bromine bromite, BrOBrO. All structures are more stable than two separated BrO molecules and could in principle be formed by the BrO + BrO reaction. They are less stable than O_2 + Br_2 in their electronic ground states. It is interesting to note here that the highly unstable isomers bromyl bromide and bromine bromite were observed for the first time in 2006 by Grothe and coworkers[44] in an argon matrix by means of IR spectroscopy. They were produced by passing a mixture of Br_2/O_2/Ar through a microwave discharge. Dibromine peroxide was not observed. As to computational work, Guha and Francisco,[39] in 1997, published a profound analysis of these molecules based on DFT calculations. Two years later, Gomez and Pácios[40,41] investigated them using MP2 *ab initio* calculations with a spin-averaged relativistic effective core potential, AREP. Papayannis and coworkers[42] used MP2 theory, with the 6-311+G(2d) basis set, and constructed a full, six-dimensional potential energy surface. The reaction dynamics was investigated by quasi-classical trajectory calculations and the rate constants k_{1a}, k_{1b} were computed. They agree well with the experimental results of Mauldin *et al.*[27] and of Harwood *et al.*[33] The dominant pathway leads to O_2 + 2Br (channel a), followed by Br_2 + O_2 (channel b). Formation of BrOOBr (channel c) was not found. In a second publication, Papayannis and Kosmas[47] studied the effect of initial vibrational excitation of BrO, which they found is minor. Furthermore, they suggested that the excited complex on the passage to the channel-b products is the planar *cis*-conformer of BrOOBr. Z. Li and Jeong[43] reported *ab initio* results using the QCISD(T)/6-311+G(2d) method. Y. Li and Vo[45] examined stationary points on the electronic ground state surface at the CCSD(T)/aug-cc-pVTZ level of theory and also reported vertical excitation energies to singlet and triplet excited states using CASSCF and MRCI. Finally, Dixon and coworkers[46] investigated a significant number of halogen–oxygen compounds at a very high level of *ab initio* theory, CCSD(T) with extrapolation to the complete basis set limit, and reported accurate thermochemical data.

To conclude, the thermochemistry of chemical reactions involving bromine oxides is now well understood. There are some open questions concerning the formation of BrOOBr and possible intermediates during the BrO + BrO self-reaction at low temperatures and pressures. The photochemistry of dibromine peroxide is completely unknown and will be investigated in the present work. We have also found a metastable van der Waals complex, $Br_2 \cdot O_2$, that might be a candidate for the four-centre intermediate postulated by Sander and Watson.[22]

2. The ground state of BrOOBr

Dibromine peroxide has a twisted equilibrium structure similar to dihydrogen peroxide. There are two enantiomeric forms, separated by torsional barriers denoted as *cis* and *trans* barriers. A detailed analysis of the torsional motion can be found in a publication by Pacios and Gómez.[40] Although these three stationary points on the electronic ground state surface were investigated by a number of groups as summarised in the introduction, consistent high-level CCSD(T)/AVTZ data, *i.e.* structures and harmonic frequencies, are not available for all of them. Furthermore, some of the data reported by Li and Vo[45] differ from those of other researchers. Consolidating calculations were thus performed in the present work, and the energies and frequencies are shown in Tables 1 and 2 to make this work self-contained. DFT(M06-2X and B3PW91)/AVTZ results are included for comparison, as DFT methods were used in the course of this work to investigate photodynamic processes.

We identified another minimum that has not been reported previously. It corresponds to a van der Waals complex, $O_2(a^1\Delta_g) \cdot Br_2(X^1\Sigma_g^+)$, located 1.2 mE$_h$ below the twisted structure. Description of the van der Waals complex requires the use of at least a triple-zeta basis set and inclusion of dynamic correlation. Without this, the computed energy will be above that of the

Table 1 Structural parameters (bond lengths in Å and angles in degrees), electronic energies and vibrational zero-point energies (in Hartree) of stationary points of BrOOBr obtained at CCSD(T), M06-2X and B3PW91 levels of theory, all with the AVTZ basis set

Structure	Method	r(BrO)	r(OO)	∠(BrOO)	τ(BrOOBr)	Energies (E_h)	ZPE (mE_h)
Twisted	M06-2X	1.839	1.378	110.70	83.12	−5298.738854	6.860
	B3PW91	1.896	1.339	112.71	84.18	−5298.687352	6.202
	CCSD(T)	1.877	1.402	110.32	83.80	−5295.382758	5.947
cis	M06-2X	1.802	1.456	118.60	0.0	−5298.721637	6.258
	B3PW91	1.800	1.501	117.80	0.0	−5298.669302	5.641
	CCSD(T)	1.812	1.548	116.88	0.0	-5295.367089	5.285
trans	M06-2X	1.808	1.449	104.61	180.0	−5298.731389	6.575
	B3PW91	1.815	1.476	104.43	180.0	−5298.676993	5.880
	CCSD(T)	1.827	1.503	103.44	180.0	−5295.375609	5.653

Table 2 Harmonic frequencies (in cm^{-1}) of the structures in Table 1 and their assignments (ν_1: torsion, ν_2: BrOO symmetric bending, ν_3: BrOO anti-symmetric bending, ν_4: BrO symmetric stretching, ν_5: BrO anti-symmetric stretching, ν_6: OO stretching)

Structure	Method	ν_1	ν_2	ν_3	ν_4	ν_5	ν_6
Twisted	M06-2X	88.60	298.08	411.35	639.56	667.59	905.90
	B3PW91	80.22	271.91	370.75	534.44	585.85	879.02
	CCSD(T)	78.35	264.05	364.55	544.35	589.10	770.15
cis	M06-2X	238.96*i*	148.28	395.80	608.03	780.34	814.39
	B3PW91	232.10*i*	133.33	384.64	585.25	617.51	755.19
	CCSD(T)	203.21*i*	136.23	359.51	508.48	592.83	722.97
trans	M06-2X	53.60	209.59	226.39	686.50	780.58	929.32
	B3PW91	38.26*i*	182.73	213.06	644.09	703.10	838.18
	CCSD(T)	25.09*i*	181.64	205.69	627.04	696.78	770.32

Table 3 Absolute and relative energies (in Hartree) of stationary points computed at CCSD(T)/AVTZ and CCSD(T)-DK/AVTZ-DK levels of theory

	CCSD(T)		CCSD(T)-DK	
Structure	Energy	Relative energy	Energy	Relative energy
cis	−5295.367090	0.016921	5359.575030	0.017340
trans	−5295.375610	0.008401	−5359.583601	0.008769
Twisted	−5295.382758	0.001253	−5359.591318	0.001061
van der Waals	−5295.384011	0.0	−5359.592372	0.0

twisted structure. The results obtained with the CCSD(T) method are presented in Table 3. Inclusion of scalar relativistic effects within the Douglas–Kroll approximation[48] do not change the results significantly.

3. UV-vis excitation of BrOOBr

BrOOBr possesses a large number of excited electronic states that can be reached from the electronic ground state by absorption of radiation with $\lambda > 300$ nm, which is the wavelength range relevant for atmospheric photochemistry. These states can be constructed by recombination of two BrO molecules in their electronic ground states $X^2\Pi$ or with one of them in the first excited state BrO ($A^2\Pi$), which is located only about 27 500 or 0.125 = 3.41 eV above the ground state.[49,50] Relativistic effects are not important for the discussion. The combination of two $^2\Pi$ states gives rise to the following electronic states of BrOOBr: two $^{1,3}\Sigma$ and $^{1,3}\Delta$, in the linear configuration. Upon bending, the degenerate D states decompose into states with symmetry $A \oplus B$ in the C_2 point group. There are thus as many as four electronic states, $3A + B$, with singlet multiplicity with asymptotes BrO($X^2\Pi$) + BrO($X^2\Pi$) or BrO($X^2\Pi$) + BrO($A^2\Pi$) and the same number of triplet states. All excited states are repulsive.

In the electronic ground state, the 86 electrons of dibromine peroxide occupy 22 orbitals of symmetry *a* and 21 orbitals of symmetry *b*. The 7 lowest excited states are generated by excitations from the three orbitals HOMO (21b), HOMO−1 (22a) and HOMO−2 (21a) to the orbitals LUMO (23a) and LUMO+1 (22b), which are shown in Fig. 1. Of these orbitals, the HOMO, HOMO−2 and HOMO−3 have major atomic orbital contributions from the bromine atoms and thus have non-bonding character. The remaining orbitals in the figure are antibonding. The electronic configurations of the excited states, generated by the promotion of electrons from non-bonding to antibonding orbitals as detailed in Table 4, indicate that these states are indeed unbound.

The high density of electronic states makes the investigation of the photodynamics a formidable task, and the choice of the quantum-chemical method is not evident *a priori*. Both *ab initio* and density functional methods were tested, with basis sets of augmented triple-zeta quality. Table 5 gives a comparison of results obtained with DFT and *ab initio* methods without consideration of relativistic corrections. The effect of the latter is minor, as can be seen from the results in Table 6, obtained at the MCSCF and MRCI levels of theory using the Douglas–Kroll[48,51] approach.† Inclusion of dynamic correlation is more important as it lowers the transition energies by about 0.2 eV (see Table 7). Li and Vo,[45] who investigated the excited electronic states previously, arrived at the same conclusion though some of their numerical data differ from ours. These differences are due to small differences in the reference configuration of the

† Molpro-recommended option DKHO = 8 with exponential parametrisation for unitary transformations.

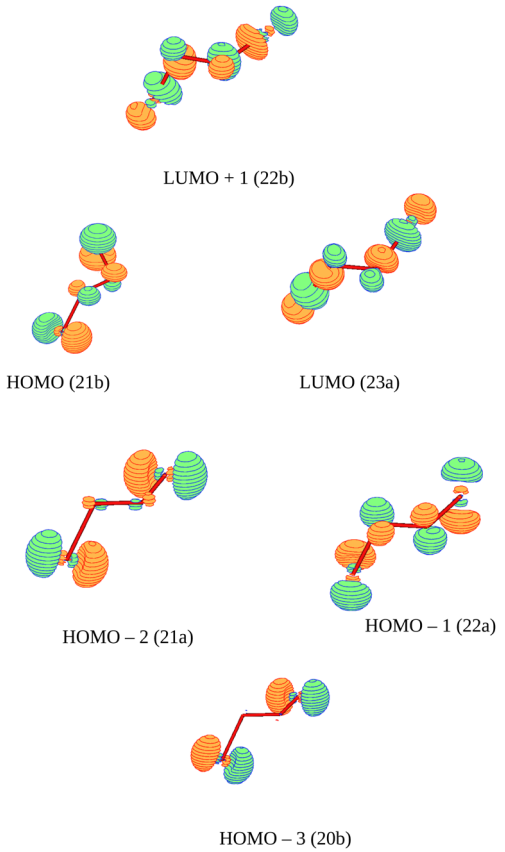

Fig. 1 Molecular orbitals of BrOOBr.

Table 4 Excitations from the electronic ground state and transition amplitudes, in %, computed at the TDDFT-TDA/AVTZ level of theory. The HOMO is orbital 21b, and the LUMO is 23a. The transition amplitudes may be positive or negative. Taking the $S_0(X^1A) \rightarrow S_1(1^1B)$ excitation as an example, the wavefunction of the $S_1(1^1B)$ electronic state is approximately described by making the excitations $0.515[\psi_{HOMO-1} \rightarrow \psi_{LUMO+1}] + 0.479[\psi_{HOMO} \rightarrow \psi_{LUMO}]$ from the $S_0(X^1A)$ electronic configuration

Transition	Orbitals	Amplitudes
$S_0(X^1A) \rightarrow S_1(1^1B)$	22a → 22b	51.5
	21b → 23a	47.9
$S_0(X^1A) \rightarrow S_2(1^1A)$	22a → 23a	48.6
	21b → 22b	50.8
$S_0(X^1A) \rightarrow S_3(2^1A)$	22a → 23a	49.5
	21b → 22b	−48.4
$S_0(X^1A) \rightarrow S_4(2^1B)$	21a → 22b	50.5
	22a → 22b	−33.9
	21b → 23a	33.8
$S_0(X^1A) \rightarrow S_5(3^1A)$	20b → 22b	39.3
	21a → 23a	58.5
$S_0(X^1A) \rightarrow S_6(3^1B)$	20b → 23a	57.0
	21a → 22b	22.8
	22a → 22b	23.5
	21b → 23a	−24.9
$S_0(X^1A) \rightarrow S_7(4^1A)$	20b → 22b	58.2
	21a → 23a	−39.1

nuclei. BrOOBr is an extremely floppy molecule, and small variations of the nuclear geometry parameters lead to notable changes in the vertical excitation energies.

Table 5 Vertical excitation energies (in eV) from the electronic ground state $S_0(X^1A)$ computed at B3PW91(TDA)/AVTZ, B3PW91(TDDFT)/AVTZ and CASSCF/AVTZ levels of theory

			CASSCF	
Excited state	B3PW91(TDA)	B3PW91(TDDFT)	Active space (26e, 16o)	Active space (26e, 18o)
$S_1(1^1A)$	3.133	3.056	3.631	3.571
$S_2(1^1B)$	3.134	3.060	3.678	3.941
$S_3(2^1A)$	3.702	3.642	4.476	4.452
$S_4(2^1B)$	3.927	3.848	4.495	4.593
$S_5(3^1A)$	3.983	3.899	4.546	4.628
$S_6(3^1B)$	4.045	3.959	5.182	5.226
$S_7(4^1A)$	4.344	4.329	5.328	5.337

Table 6 Comparison of vertical excitation energies (in eV) obtained with the *ab initio* methods MCSCF (CAS(26e, 16o)), MRCI based on the same CAS, with and without relativistic corrections and EOM–CCSD, mostly with the AVTZ basis set. Relativistic effects were treated with the Douglas–Kroll Hamiltonian, $MCSCF^{DK}$, or with the def2-TZVP effective core potential for bromine, $MCSCF^{ECP}$

	MCSCF			MRCI		
Excited state	MCSCF	$MCSCF^{DK}$	$MCSCF^{ECP}$	MRCI	$MRCI^{DK}$	EOM–CCSD
$S_1(1^1A)$	3.631	3.594	3.595	3.436	3.399	3.274
$S_2(1^1B)$	3.678	3.637	3.637	3.470	3.433	3.305
$S_3(2^1A)$	4.476	4.421	4.423	4.204	4.158	4.147
$S_4(2^1B)$	4.495	4.438	4.441	4.266	4.216	4.155
$S_5(3^1A)$	4.546	4.495	4.495	4.277	4.228	4.802
$S_6(3^1B)$	5.182	5.128	5.128	5.007	4.972	4.909
$S_7(4^1A)$	5.328	5.271	5.271	5.240	5.187	5.445

The tables demonstrate that the outcomes from different methods differ in particular for excitation to higher electronic states. It should be noted, however, that the vertical transition energies and oscillator strengths can only give a crude approximation to the UV spectrum of the title molecule, as this can depart significantly from the equilibrium nuclear configurations due to large-amplitude torsional motion. For a more realistic simulation of the UV spectrum, displacement of the nuclei from their equilibrium positions needs to be taken into account. Such a simulation was performed using the Newton-X package[52] coupled to Gaussian G16[53] or to Molpro.‡[54] Within Newton-X, the photoabsorption cross section is computed as

$$\sigma(\lambda) = \frac{\pi e^2}{2m_e c\varepsilon_0} \sum_{l \neq i}^{N_{fs}} \left[\frac{1}{N_p^l} \sum_{k}^{N_p^l} f_{il}(\mathbf{x}_k) g(E - \Delta E_{il}(\mathbf{x}_k), \delta) \right] \quad (5)$$

with e being the elementary charge, m_e the electron mass, c the speed of light and ε_0 the vacuum permittivity. $E = hc/\lambda$ is the radiation energy. f_{il} is the oscillator strength for transitions between the initial electronic state i and the final state l, and ΔE_{il} is the corresponding transition energy, and summation is made over final excited states. The other sum samples the

‡ A Molpro–Newton-X interface was provided by Alex Brown and Zhibo Wang,[55] and extended by the present authors.

Table 7 Comparison of excitation energies and oscillator strengths for excitation from the electronic ground state $S_0(X^1A)$ for three selected methods

	B3PW91(TDA)			MCSCF, CAS(26e, 16o)			MRCI		
Excited	E (eV)	λ (nm)	f	E (eV)	λ (nm)	f	E (eV)	λ (nm)	f
$S_1(1^1A)$	3.133	395.70	0.0001	3.631	341.46	0.0008	3.436	360.79	0.0000
$S_2(1^1B)$	3.134	395.60	0.0000	3.678	337.46	0.0010	3.470	357.26	0.0001
$S_3(2^1A)$	3.702	334.88	0.0077	4.476	277.18	0.0050	4.204	294.91	0.0064
$S_4(2^1B)$	3.927	315.72	0.0440	4.495	275.94	0.0017	4.266	290.59	0.0003
$S_5(3^1A)$	3.983	311.21	0.0000	4.546	272.97	0.0028	4.277	289.85	0.0003
$S_6(3^1B)$	4.045	306.45	0.0324	5.182	239.49	0.0459	5.007	247.61	0.0466
$S_7(4^1A)$	4.344	285.42	0.0005	5.328	232.92	0.0013	5.240	236.59	0.0006

nuclear configurations, $\mathbf{x}_k$, which are obtained as deviations from a reference configuration along the normal modes and weighted by a Wigner distribution. Finally, g is a Gaussian lineshape function with a broadening of δ = 0.06 eV to remove statistical noise, as described in detail by Barbatti *et al.*[56]

Using Newton-X software, the UV-vis spectrum was computed employing a variety of quantum chemical methods, with the aim to determine the most adequate procedure for the investigation of photodynamics. The strategy adopted previously[57] by our group is that the method that reproduces the experimental spectrum best should also be reliable away from the Franck–Condon region and thus appropriate for photodynamics. Both MCSCF and TDDFT methods are computationally feasible for use in photodynamics and were tested here, and some of the results are presented in Fig. 2 where they are compared with the experimental spectrum.[27,33] It can be seen that the signal obtained with MCSCF is quite displaced from the experimental one, whereas TDDFT/B3PW91 leads to almost perfect agreement, as far as both position and intensity are concerned.

The decomposition of the computed UV spectrum in terms of electronic states is presented in Fig. 3. Contributions are due to excitations to the seven lowest singlet states, but that from the first excited state is negligible over the entire range of wavelengths. An important contribution comes from the fifth excited state, though the oscillator strength corresponding to vertical excitation from the ground state equilibrium nuclear configuration is zero. This is a manifestation of large-amplitude motion and demonstrates the importance of adequate sampling of nuclear configurations.

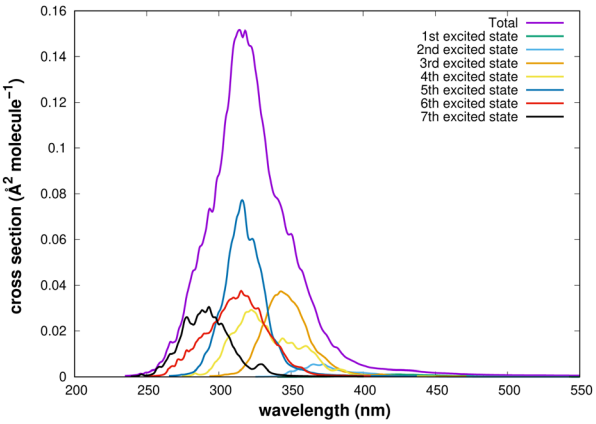

Fig. 3 UV spectrum computed with the B3PW91(TDA)/AVTZ method and its contributions from individual electronic states.

The same spectrum computed at the MCSCF/AVTZ level (Fig. 4) is blue-shifted from the DFT spectrum. Furthermore, there are differences in the excited state contributions, mainly that there is now a strong absorption to the S_7 state rather than to the S_5 state of the DFT calculation, which we attribute to differences in the orbital energies. The MCSCF spectrum could have been improved by inclusion of dynamic correlation by

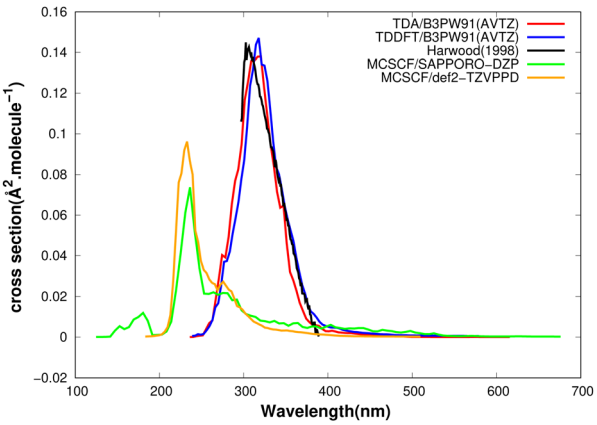

Fig. 2 Comparison between theoretical and experimental UV spectra.

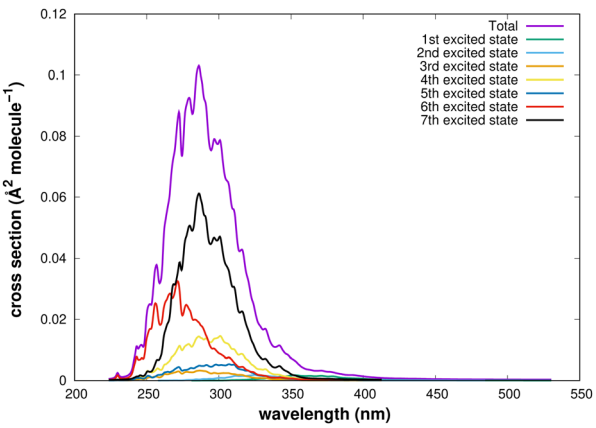

Fig. 4 UV spectrum computed with the MCSCF/AVTZ method and its contributions from individual electronic states.

means of a MRCI calculation. Such a treatment is expected to shift the signal by about 0.2 eV towards the red, judging from the results presented in Table 6, but it would still be displaced from the experimental spectrum. As the DFT result is very satisfying, we did not compute the spectrum at the MRCI level of theory.

4. Photodecomposition of excited BrOOBr

4.1. Product channels

The photodecomposition of dibromine peroxide was studied by running classical trajectories using the Newton-X package. For each of the excited electronic states, 150 trajectories were followed up to a simulation time of t_{max} = 1000 fs with step size Δ_t = 0.5 fs. The initial conditions for the trajectories were obtained by projecting a sample of nuclear configurations from the ground state surface to that of an excited state and computing their initial velocities from the derivatives of the potential energy surface. Electronic energies, gradients and non-adiabatic coupling terms were computed on the fly using the Gaussian G16 quantum chemistry code. The TDDFT-TDA/B3PW91 approach was used with the AVTZ basis set.

Three product channels can be distinguished, leading to 2BrO (channel a), BrOO + Br (channel b) or 2Br + O_2 (channel c). BrOO was observed experimentally[58,59] but is highly unstable[60] and, if initially formed photochemically, would likely decompose into Br + O_2. However, it may also be produced by thermal decomposition of ground state BrOOBr at low temperatures. The excited states of BrOO are repulsive. Table 8 provides the possible exit channels for each of the excited electronic states, including S_1 though it is not populated, and an estimate of their asymptotic energies. The latter were computed using the data from ref. 46 and 49.

The results of the trajectory calculations are presented in Table 9. For the automatic identification of the fragments, we consider a bond as broken when its internuclear distance exceeds the initial value by more than 25%. The procedure was adopted in a previous work on photodynamics.[61] The formation probabilities p and error bounds were obtained by a statistical analysis as $p \pm zp(1-p)/n$, with p being the fraction of trajectories leading to a particular fragment channel and n the total number of trajectories. z = 1.96 for the 95% confidence interval. The error bounds for the 2BrO channel are as large as the formation probabilities as only very few trajectories lead to these products. One trajectory is analysed in detail in Fig. 5 and the explanatory text in Section 4.2.

Table 8 Photochemical product channels and asymptotic energies. BrOO is very weakly bound in its electronic ground state. The excited states are repulsive

States	Products	E (eV)	Products	E (eV)
Channel BrOOBr → 2BrO				
S_0–S_3	2BrO ($X^2\Pi$)			0.950
S_4–S_7	BrO ($X^2\Pi$) + BrO ($A^2\Pi$)			4.360
Channel BrOOBr → BrOO + Br → 2Br + O_2				
S_0–S_2	BrOO (X^2A'') + Br (^2P)	0.690	2Br (^2P) + O_2 ($X^3\Sigma_g^-$)	0.600
S_3–S_6	BrOO (A^2A') + Br (^2P)	—	2Br (^2P) + O_2 ($X^3\Sigma_g^-$)	0.600
S_7–S_{10}	BrOO (B^2B') + Br (^2P)	—	2Br (^2P) + O_2 ($X^1\Delta$)	1.577

Table 9 Fragment statistics of the trajectories as a function of the initial excited electronic state. The S_1 state was omitted as it is not populated. The fragments were determined at a propagation time of up to 1000 fs. BrOO in the last column will decompose into Br + O_2

State	BrO + BrO	2Br + O_2	Br + BrOO
S_2	0.01 ± 0.01	0.40 ± 0.07	0.59 ± 0.07
S_3	0.02 ± 0.02	0.69 ± 0.07	0.29 ± 0.07
S_4	0.00	0.81 ± 0.06	0.19 ± 0.06
S_5	0.00	0.79 ± 0.06	0.16 ± 0.05
S_6	0.00	0.82 ± 0.06	0.18 ± 0.06
S_7	0.00	0.96 ± 0.03	0.04 ± 0.03

Performing the trajectory calculations for dibromine peroxide is challenging even on a supercomputer. It is computationally prohibitive to follow the trajectories over a sufficient time interval for the formation of the final fragments as the non-adiabatic dynamics of BrOOBr is slow because of the heavy bromine nuclei. What is more, the need to include up to seven electronic states in the simulation requires small time steps to assure numerical stability. The Tamm–Dancoff approximation to the time-dependent density functional approach was used here as it performs favourably well, particularly in the asymptotic region where the electronic states are dense and avoided crossings are common.[62] However, not all trajectories could be propagated up to the end due to numerical instabilities. In those cases, the dissociation products were analysed manually at the last point of the propagation.

4.2. Mechanisms of photodecomposition

The principal reaction channel is the one leading to 2Br + O_2 in their electronic ground states. Two distinct mechanisms are present: concerted rupture of the two Br–O bonds or sequential rupture. Concerted rupture occurs mainly on highly excited electronic state surfaces, S_3 or higher. On the lower electronic states, S_0 to S_2, sequential rupture is favoured as the BrOO (X^2A'') fragment is weakly bound. The second bond then breaks up within 50 fs after the first bond. The fragment distribution in Table 9 reflects the result of a competition between fast breakup followed by non-adiabatic stabilisation and the opposite, *i.e.* rapid non-adiabatic relaxation and breakup on a lower electronic surface.

There is also a certain probability of separation into two BrO radicals. This is a rare event as the O–O bond is much stronger than the Br–O bond. The mechanism for such a breakup is quite remarkable. It can be identified from Fig. 5 where the time evolution of the internuclear distances is shown for the case of BrOOBr initially placed on the S_2 electronic surface. Fast oscillations of the O–O bond are observed along with slow oscillations, with a period of about 400 fs, corresponding to a frequency of 76, which is due to large-amplitude torsional motion. During the first period, the Br–O bonds vibrate in phase. Thus, the Br–O bond lengths augment significantly, up to 2.8 Å. It is quite remarkable that the bromine atoms do

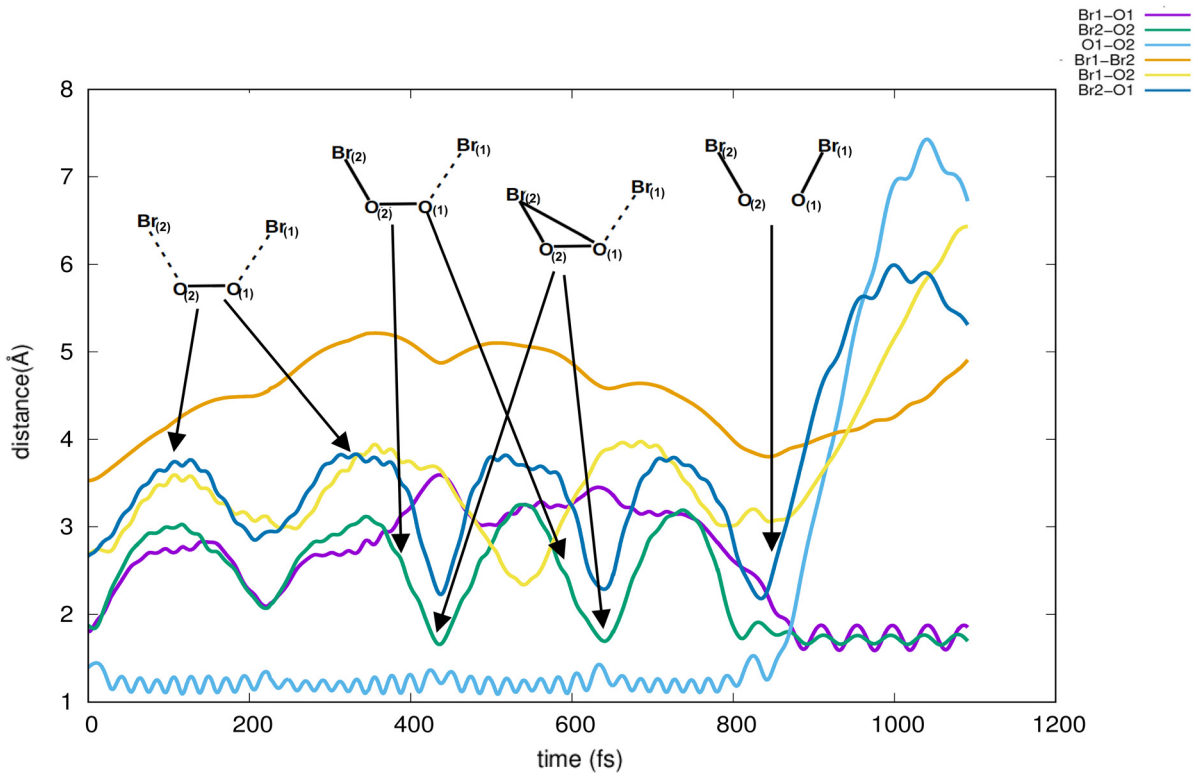

Fig. 5 Time evolution of internuclear distances on a trajectory leading to breakup of the O–O bond.

not fly apart but rather reapproach their oxygen atoms. During the second period, between 400 fs and 800 fs, the Br–O bonds oscillate out of phase. It can be noted that, at the beginning of this phase, the bromine atom labelled $Br_{(1)}$ arrives at a distance of about 3.5 Å from oxygen $O_{(1)}$, violet line in the figure, and then keeps a distance of about 3 Å over 300 fs, while the remaining triatomic fragment undergoes several rearrangements, with intermediate triatomic structures resembling bromine peroxide BrOO and bromine dioxide OBrO. Then, suddenly, $Br_{(1)}$ approaches its oxygen atom and at about 800 fs the O–O bond breaks up. The two BrO fragments separate. During this second period, near 760 fs, a non-adiabatic transition from S_2 to S_1 takes place and electronic energy is converted to vibrational energy. Another non-adiabatic transition occurs at 880 fs where the system arrives on the electronic ground state.

The breakup of the O–O bond is thus a result of energy transfer from electronic to nuclear motion followed by intramolecular vibrational energy redistribution towards the O–O vibration, though it appears more accurate to classify this as intermolecular vibrational energy redistribution, given that the bromine atoms are at large distances while the dioxygen keeps vibrating. The dissociation process is slow as it passes through a complex vibronic resonance.

4.3. Dissociation rate constant

The unimolecular photodecomposition rate constant J can be computed as

$$J = \sum_A \int F(\lambda)\sigma(\lambda)\varphi_A(\lambda)\mathrm{d}\lambda \qquad (6)$$

where $F(\lambda)$ is the actinic flux,§ $\sigma(\lambda)$ the absorption cross section and $\phi_A(\lambda)$ the quantum yield for the formation of product A. In the present case, we only have one dissociation channel and hence $\phi(\lambda) = 1$. The value of the decay constant is

$$J = 9.7 \times 10^{-2}\ \mathrm{s}^{-1} \qquad (7)$$

This constant may be compared with the rate constant of thermal decomposition reported by Harwood *et al.*[33] at temperatures of $T_1 = 222$ K and $T_2 = 235$ K. For the second-order decomposition

$$\frac{\mathrm{d[BrOOBr]}}{\mathrm{d}t} = -k_{-1}[\mathrm{M}][\mathrm{BrOOBr}] \qquad (8)$$

in the presence of ozone as collider M, the rate constants are $k_{-1}(222\ \mathrm{K}) = (2.5 \pm 0.5) \times 10^{-18}$ cm^3 molecule^{-1} s^{-1} and $k_{-1}(235\ \mathrm{K}) = (5.8 \pm 3.0) \times 10^{-18}$ cm^3 molecule^{-1} s^{-1}. Typical ozone concentrations in the experiment are between 5×10^{18} molecules cm^{-3} and 25×10^{18} molecules cm^{-3}, from which the unimolecular decay constant $k_{-1}^{\mathrm{uni}} = k_{-1}/[\mathrm{M}]$ can be roughly estimated as

$$k_{-1}^{\mathrm{uni}} \approx 10^{-1}\ \mathrm{s}^{-1} \qquad (9)$$

The density of potential collider molecules near the tropopause is of the same order, so that in view of atmospheric chemistry the two decay mechanisms are equally important.

§ The National Center for Atmospheric Research in Boulder (https://www.acom.ucar.edu/Models/TUV/Interactive_TUV/)

5. Conclusions

Dibromine peroxide is a weakly stable molecule whose very existence and formation in a termolecular reaction, *i.e.* recombination of two BrO radicals in the presence of a third body, M, was proved indirectly by the well-known experiments conducted by Mauldin[27] and Harwood[33] and their colleagues some time ago. They have particularly shown that this molecule is stable at temperatures below 250 K, which are typically found in the Earth's atmosphere near the tropopause. Rate constants for its formation and thermal decomposition are well reported in the literature, as outlined in the introduction. In contrast, the photochemistry of dibromine peroxide has remained unexplored, despite the importance of photochemical reactions in the atmosphere in general. We have shown in the present work, by means of mixed quantum–classical trajectory calculations on seven coupled electronic potential energy surfaces, that photoexcited dibromine peroxide decomposes rapidly ($\tau_{1/2} \approx 7$ s), eventually leading, *via* different unstable intermediates, to $2Br + O_2$, which are also the principal thermal decomposition products. The rate constant for photodecomposition under atmospheric conditions was estimated as $J = 9.7 \times 10^{-2}$ s^{-1} and is comparable to the thermal decomposition rate constant. Therefore, photolysis should be taken into account in atmospheric modelling as it likely affects the Br/BrO ratio. We finally conclude that bromine containing radicals (Br and BrO) are not neutralised by the BrOOBr channel and remain active species in the atmosphere.

The mechanism leading to the breakup into two BrO radicals following vibronic energy redistribution is most uncommon, and we are not aware of similar processes in molecular physics. We therefore hope that our results will lead to new experiments aiming at a better understanding of the formation and decomposition of dibromine peroxide, particularly since the two less stable isomers of Br_2O_2 were observed experimentally in 2006 by Grothe and coworkers.[44]

Author contributions

All authors contributed equally to this work. W. C. is a PhD student supervised by the other three authors.

Conflicts of interest

There are no conflicts to declare.

Data availability

All data are reported in the article. The following computational codes were used: 1. Gaussian G16, 2. Molpro and 3. Newton-X. They were all cited in the article.

Acknowledgements

We are grateful for the financial support from the ''PHC Utique'' programme of the French Ministry of Foreign Affairs and Ministry of Higher Education and Research and the Tunisian Ministry of Higher Education and Scientific Research (project number 24G1301). W. C. acknowledges a PhD studentship from the Tunisian Ministry of Higher Education and Scientific Research. The supercomputer time was provided by the ROMEO HPC Center at the University of Reims Champagne-Ardenne, by CRIANN (Centre des Ressources Informatiques et Applications Numériques de Normandie) and by GENCI-IDRIS (Grant 2024-103918).

Notes and references

1 M. J. Molina and F. S. Rowland, *Nature*, 1974, **249**, 810–812.
2 L. T. Molina and M. J. Molina, *J. Phys. Chem.*, 1987, **91**, 433–436.
3 T. von Clarmann, *Atmosfera*, 2013, **26**, 415–458.
4 D. J. Lary, *J. Geophys. Res.*, 1997, **102**, 21515–21526.
5 J. J. Lin, A. F. Chen and Y. T. Lee, *Chem. – Asian J.*, 2011, **6**, 1664–1678.
6 J. B. Burkholder, R. A. Cox and A. R. Ravishankara, *Chem. Rev.*, 2015, **115**, 3704–3759.
7 J. S. Daniel, S. Solomon, R. W. Portmann and R. R. Garcia, *J. Geophys. Res.*, 1999, **104**, 23871–23880.
8 B.-M. Sinnhuber, N. Sheode, M. Sinnhuber, M. P. Chipperfield and W. Feng, *Atmos. Chem. Phys.*, 2009, **9**, 2863–2871.
9 J. E. Klobas, D. K. Weisenstein, R. J. Salawitch and D. M. Wilmouth, *Atmos. Chem. Phys.*, 2020, **20**, 9459–9471.
10 G. Le Bras and U. Platt, *Geophys. Res. Lett.*, 1995, **22**, 599–602.
11 Y. Bedjanian and G. Poulet, *Chem. Rev.*, 2003, **103**, 4639–4656.
12 R. J. Salawitch, M. B. McElroy, J. H. Yatteau, S. C. Wofsy, M. R. Schoeberl, L. R. Lait, P. A. Newman, K. R. Chan, M. Loewenstein, J. R. Podolske, S. E. Strahan and M. H. Proffitt, *Geophys. Res. Lett.*, 1990, **17**, 561–564.
13 J. G. Anderson, D. Toohey and W. H. Brune, *Science*, 1991, **251**, 39–46.
14 M. B. McElroy, R. J. Salawitch, S. C. Wofsy and J. A. Logan, *Nature*, 1986, **321**, 759–762.
15 J. McConnell, G. Henderson, L. Barrie, J. Bottenheim, H. Niki, C. Langford and E. Templeton, *Nature*, 1992, **355**, 150–152.
16 T. K. Koenig, S. Baidar, P. Campuzano-Jost, C. A. Cuevas, B. Dix, R. P. Fernandez, H. Guo, S. R. Hall, D. Kinnison, B. A. Nault, K. Ullmann, J. L. Jimenez, A. Saiz-Lopez and R. Volkamer, *Proc. Natl. Acad. Sci. U. S. A.*, 2020, **117**, 1860–1866.
17 C. A. Cuevas, R. P. Fernandez, D. E. Kinnison, Q. Li, J.-F. Lamarque, T. Trabelsi, J. S. Francisco, S. Solomon and A. Saiz-Lopez, *Proc. Natl. Acad. Sci. U. S. A.*, 2022, **119**, e2110864119.
18 P. Ricaud and F. Lefèvre, Advances in Fluorine Science, in *Fluorine and the Environment*, ed. A. Tressaud, Elsevier, 2006, vol. 1, pp. 1–32.

19 W. H. Schlesinger, E. M. Klein and A. Vengosh, *Global Biogeochemical Cycles*, 2020, **34**, e2020GB006722.
20 M. A. Clyne and R. T. Watson, *J. Chem. Soc., Faraday Trans. 1*, 1975, **71**, 336–350.
21 S. Jaffe and W. Mainquist, *J. Phys. Chem.*, 1980, **84**, 3277–3280.
22 S. P. Sander and R. T. Watson, *J. Phys. Chem.*, 1981, **85**, 4000–4007.
23 R. Cox, D. Sheppard and M. Stevens, *J. Photochem.*, 1982, **19**, 189–207.
24 A. A. Turnipseed, J. W. Birks and J. G. Calvert, *J. Phys. Chem.*, 1990, **94**, 7477–7482.
25 I. Barnes, V. Bastian, K. Becker and R. Overath, *Int. J. Chem. Kinet.*, 1991, **23**, 579–591.
26 I. Lancar, G. Laverdet, G. L. Bras and G. Poulet, *Int. J. Chem. Kinet.*, 1991, **23**, 37–45.
27 R. Mauldin III, A. Wahner and A. Ravishankara, *J. Phys. Chem.*, 1993, **97**, 7585–7596.
28 I. Bridier, B. Veyret and R. Lesclaux, *Chem. Phys. Lett.*, 1993, **201**, 563–568.
29 D. M. Rowley, M. H. Harwood, R. A. Freshwater and R. L. Jones, *J. Phys. Chem.*, 1996, **100**, 3020–3029.
30 M. K. Gilles, A. A. Turnipseed, J. B. Burkholder, A. Ravishankara and S. Solomon, *J. Phys. Chem. A*, 1997, **101**, 5526–5534.
31 B. Laszlo, R. E. Huie, M. J. Kurylo and A. W. Miziolek, *J. Geophys. Res.*, 1997, **102**, 1523–1532.
32 Y. Bedjanian, G. Le Bras and G. Poulet, *J. Phys. Chem. A*, 1998, **102**, 10501–10511.
33 M. H. Harwood, D. M. Rowley, R. A. Cox and R. L. Jones, *J. Phys. Chem. A*, 1998, **102**, 1790–1802.
34 V. Ferracci, K. Hino and D. M. Rowley, *Phys. Chem. Chem. Phys.*, 2011, **13**, 7997–8007.
35 M. K. M. Ward and D. M. Rowley, *Phys. Chem. Chem. Phys.*, 2017, **19**, 23345–23356.
36 Y. Bedjanian, *Int. J. Chem. Kinet.*, 2020, **52**, 319–328.
37 G.-N. Porter, *Proc. R. Soc. London, Ser. A*, 1950, **200**, 284–300.
38 J. B. Burkholder, S. P. Sander, J. Abbatt, J. R. Barker, *et al.*, Chemical Kinetics and Photochemical Data for Use in Atmospheric Studies, Evaluation No. 19, Publication 19-5, Pasadena, ca: Jet propulsion laboratory, national aeronautics and space technical report, 2019.
39 S. Guha and J. S. Francisco, *J. Phys. Chem. A*, 1997, **101**, 5347–5359.
40 L. Pacios and P. Gómez, *THEOCHEM*, 1999, **467**, 223–231.
41 P. C. Gómez and L. F. Pacios, *J. Phys. Chem. A*, 1999, **103**, 739–743.
42 D. Papayannis, A. M. Kosmas and V. S. Melissas, *Chem. Phys.*, 1999, **243**, 249–262.
43 Z. Li and G.-R. Jeong, *Chem. Phys. Lett.*, 2001, **340**, 194–204.
44 O. Gálvez, A. Zoermer, A. Loewenschuss and H. Grothe, *J. Phys. Chem. A*, 2006, **110**, 6472–6481.
45 Y. Li and C. K. Vo, *J. Chem. Phys.*, 2006, **124**, 204309.
46 D. J. Grant, E. B. I. Garner, M. H. Matus, M. T. Nguyen, K. A. Peterson, J. S. Francisco and D. A. Dixon, *J. Phys. Chem. A*, 2010, **114**, 4254–4265.
47 D. K. Papayannis and A. M. Kosmas, *Can. J. Chem.*, 2001, **79**, 1940–1945.
48 M. Douglas and N. M. Kroll, *Ann. Phys.*, 1974, **82**, 89–155.
49 Y. Li, J. S. Francisco and K. A. Peterson, *J. Chem. Phys.*, 2000, **113**, 8556–8560.
50 D. Zhou, D. Shi, J. Sun and Z. Zhu, *Comput. Theor. Chem.*, 2017, **1112**, 94–103.
51 T. Nakajima and K. Hirao, *Chem. Rev.*, 2012, **112**, 385–402.
52 M. Barbatti, M. Ruckenbauer, F. Plasser, J. Pittner, G. Granucci, M. Persico and H. Lischka, *Wiley Interdiscip. Rev.: Comput. Mol. Sci.*, 2014, **4**, 26–33.
53 M. J. Frisch, G. W. Trucks, H. B. Schlegel, G. E. Scuseria and M. A. Robb, *et al.*, *Gaussian 16 Revision C.01*, Gaussian Inc., Wallingford CT, 2016.
54 H.-J. Werner, P. J. Knowles, G. Knizia, F. R. Manby, M. Schütz, *et al.*, *MOLPRO, version 2021.1, a package of ab initio programs*, 2021, see **https://www.molpro.net**.
55 Z. Wang, PhD thesis, Department of Chemistry, Supervisor Alex Brown, 2019.
56 M. Barbatti, A. J. A. Aquino and H. Lischka, *Phys. Chem. Chem. Phys.*, 2010, **12**, 4959–4967.
57 O. Ferchichi, N. Derbel, T. Cours and A. Alijah, *Phys. Chem. Chem. Phys.*, 2020, **22**, 4059–4071.
58 J. Kölm, A. Engdahl, O. Schrems and B. Nelander, *Chem. Phys.*, 1997, **214**, 313–319.
59 K. Suma, Y. Sumiyoshi and Y. Endo, *J. Chem. Phys.*, 2005, **123**, 024312.
60 L. F. Pacios and P. C. Gómez, *J. Phys. Chem. A*, 1997, **101**, 1767–1773.
61 W. Chebbi, N. Derbel, A. Alijah and T. Cours, *Phys. Chem. Chem. Phys.*, 2024, **26**, 123–129.
62 S. Hirata and M. Head-Gordon, *Chem. Phys. Lett.*, 1999, **314**, 291–299.

